

SPECTROPOLARIMETRY OF R CORONAE BOREALIS IN 1998–2003: DISCOVERY OF TRANSIENT POLARIZATION AT MAXIMUM BRIGHTNESS

K. S. Kawabata^{1,2}, Y. Ikeda^{3,2}, H. Akitaya^{4,2}, M. Isogai^{1,2}, K. Matsuda⁵, M. Matsumura⁶,
O. Naga⁷, and M. Seki⁸

ABSTRACT

We present an extended optical spectropolarimetry of R CrB from 1998 January to 2003 September. The polarization was almost constant in the phase of maximum brightness, being consistent with past observations. We detected, however, temporal changes of polarization ($\sim 0.5\%$) in 2001 March and August, which were the first detection of large polarization variability in R CrB near maximum brightness. The amplitude and the position angle of the ‘transient polarization’ were almost constant with wavelength in both two events. There was a difference by about 20 degrees in the position angle between the two events. Each event could be explained by light scattering due to short-lived dust puff occasionally ejected off the line of sight. The flatness of the polarization against the wavelength suggests that the scatterer is a mixture of dust grains having various sizes. The rapid growth and fading of the transient polarization favors the phenomenological model of dust formation near the stellar photosphere (e.g., within two stellar radii) proposed for the time evolution of brightness and chromospheric emission lines during deeply declining periods, although the fading timescale can hardly be explained by a simple dispersal of expanding dust puff with a velocity of $\sim 200 - 350 \text{ km s}^{-1}$. Higher expansion velocity or some mechanism to destroy the dust grains should be needed.

Subject headings: circumstellar matter — dust, extinction — stars: individual (R Coronae Borealis) — stars: mass-loss — techniques: polarimetric

¹Hiroshima Astrophysical Science Center, Hiroshima University, 1-3-1 Kagamiyama, Higashi-Hiroshima, Hiroshima 739-8526, Japan; kawabtkj@hiroshima-u.ac.jp, isogai@hiroshima-u.ac.jp

²Visiting Astronomer, Okayama Astrophysical Observatory of National Astronomical Observatory of Japan (NAOJ)

³Photocoding, Higashi-Hashimoto 3-16-8-101, Sagamihara, Kanagawa 229-1104, Japan; ikeda@photocoding.com

⁴Division of Optical and Infrared Astronomy, NAOJ, Osawa 2-21-1, Mitaka, Tokyo 181-8588, Japan; akitaya@optik.nao.ac.jp

⁵Nishi-Harima Astronomical Observatory, Sayo-cho, Hyogo 679-5313, Japan; matsuda@nhao.go.jp

⁶Faculty of Education, Kagawa University, Saiwai-cho 1-1, Takamatsu 760-8522, Japan; matsu@ed.kagawa-u.ac.jp

⁷Department of Physical Science, School of Science, Hiroshima University, 1-3-1 Kagamiyama, Higashi-Hiroshima, Hiroshima 739-8526, Japan; naga@hep01.hepl.hiroshima-u.ac.jp

⁸Astronomical Institute, Graduate School of Science,

1. INTRODUCTION

R Coronae Borealis (RCB) stars are hydrogen-deficient, carbon-rich variables that undergo declines in visual brightness up to 7 mag or more at irregular intervals. The evolutionary pathways of these stars are still unclear, with the white dwarf merger model and the final helium-shell flash model being suggested for the extreme abundances (e.g., Iben, Tutukov, & Yungelson 1996; Saio & Jeffery 2002; Clayton et al. 2007). The darkening phenomenon has been attributed to eclipse by clouds of dust grains (dust puff) formed along the line of sight (Loreta 1934; O’Keefe 1939). Near-infrared excess, attributable to the dust emission

Tohoku University, Aramaki, Aoba-ku, Sendai 980-8578, Japan; seki@astr.tohoku.ac.jp

at an equivalent blackbody temperature of ~ 900 K, was found for the prototype of this group, R CrB (Stein et al. 1969), and this excess is a general property of RCB stars (Feast & Glass 1973). The infrared radiation shows variations on timescales of ~ 3.5 yr (Feast et al. 1997) and does not clearly correlate with the optical brightness (Forrest, Gillett, & Stein 1972; Feast et al. 1997; Yudin et al. 2002). These indicate that a large amount of dust being produced surrounds the star and that a smaller dust puff is formed in a random direction per any one ejection event (e.g., Ohnaka et al. 2001, 2003). Recent near-infrared adaptive optics observations with an 8-m class telescope directly revealed the presence of multiple dusty clouds in the vicinity of RY Sgr (de Laverny & Mékarnia 2004).

The dust formation mechanism itself is, however, still one of the fundamental problems in RCB stars (e.g., Clayton 1996; Feast 1997, 2000). Fadeyev (1986) derived from a theoretical argument a conclusion that the dust formation has to occur somewhere $\sim 20R_*$ apart from the central star where the local temperature becomes low enough to allow for carbon grains to condense. On the other hand, observational facts such as the time evolution of chromospheric emission lines and timescales of brightness recovering from declines are favorable to other models in which dust forms in close proximity ($\lesssim 2R_*$) to the central star (Clayton et al. 1992; Whitney 1993). To settle this discrepancy, some mechanism to promote dust formation near RCB stars have been proposed. Woitke, Goeres, & Sedlmayr (1996) suggested that the local gas temperature can be substantially decreased by supercooling after the passage of a shock wave driven by stellar pulsation. Asplund & Gustafsson (1996) proposed an episodic local density inversions in the ionization layer of helium due to a kind of radiative instability which can promote a blob ejection. Feast (1997) discussed the dust formation above the cool regions of giant convection cells. Soker & Clayton (1999) suggest that cool magnetic spots existing inside of photosphere facilitate dust formation above the spots after a shock wave passes.

Polarimetry is a probe sensitive to circumstellar medium near the stellar surface, and even to dust formation episodes around RCB stars on very small spatial scales. If dust forms actually near the

photosphere ($\lesssim 2R_*$), the angular size of the dust puff should be more than 50° for total eclipse of the stellar disk. Such a wide dust puff is likely to scatter the light from the star and may cause a net polarization more than 0.5–1 %, when it locates along the direction nearly orthogonal to the line of sight (Code & Whitney 1995). Therefore, it is natural to expect that RCB stars temporally show a significant polarization at maximum brightness stage. The wavelength dependence of the polarization would give unique information about the “newborn” dust grain. So far only small fluctuation of intrinsic polarization less than 0.2 % has been found for RCBs near maximum brightness (Serkowski & Kruszewski 1969; Coyne & Shawl 1973; Coyne 1974; Efimov 1980, 1990; Stanford et al. 1988; Rosenbush & Rosenbush 1990; Whitney et al. 1992; Trammell, Dinerstein, & Goodrich 1994; Clayton et al. 1995, 1997; Yudin et al. 2003; Biegging et al. 2006), except for Efimov (1980)’s observation on 1974 August 24 ($p_V = 0.38 \pm 0.03$ %).

In this paper, we present a new spectropolarimetry of R CrB on 84 nights in 1998–2003. We successfully found two events of temporal increase in polarization by about 0.5 % at maximum brightness stage. We consider the period when the visual magnitude is within 0.3 mag below the maximum V magnitude (V_{\max}) as “maximum brightness” phase and call the other period “decline” phase. We adopt $V_{\max} = 6.09$ which is the mean magnitude during the apparent visual maximum of R CrB, JD2,450,800–51,000 and 52,000–52,650 (Figure 1a). The photometric data referred in this paper are obtained from the VSNET¹ and AAVSO² databases.

2. OBSERVATIONS AND DATA REDUCTION

The data were obtained with the low-resolution spectropolarimeter, HBS (an acronym of “Henkou-Bunkou-Sokkou-Ki” which stands for spectropolarimeter in Japanese; Kawabata et al. 1999) from 1998 January 28 to 2003 September 29 at the Dodaira Observatory and the Okayama Astrophysical Observatory of NAOJ. At the Dodaira

¹Variable Star NETWORK; <http://www.kusastro.kyoto-u.ac.jp/vsnet/>

²American Association of Variable Star Observers; <http://www.aavso.org/>

Observatory, HBS was attached to the Cassegrain focus of the 0.91 m telescope ($F/18$; $12''.4 \text{ mm}^{-1}$ at the focal plane). At Okayama Astrophysical Observatory, HBS was attached to the Cassegrain focus of either the 0.91 m telescope ($F/13$; $17''.2 \text{ mm}^{-1}$) or the 1.88 m telescope ($F/18$; $6''.1 \text{ mm}^{-1}$). HBS has a superachromatic half-wave plate and a quartz Wollaston prism; the orthogonally polarized spectra are simultaneously recorded on either a front-illuminated type TI CCD (1024×1024 pixels, $12 \mu\text{m}$ square per pixel) or a back-illuminated type SITe CCD (512×512 pixels, $24 \mu\text{m}$ square per pixel). We used either the 1.4 mm circular hole (D1) or the $0.2 \text{ mm} \times 1.4 \text{ mm}$ rectangular hole (D2) as a focal diaphragm. Each diaphragm has two holes of the same dimension, and we put a target star in one hole and the nearby sky in the other. For the observations with D1 diaphragm, the spectral resolution depends on the seeing size because the stellar image size is much smaller than the diameter of the circular hole. For the observations with D2, the spectral resolution also depends on the stellar image size at the Okayama 0.91 m telescope, while it does not at the other telescopes because the stellar image size was usually larger than the narrower dimension of the rectangular hole. Nevertheless, the spectral resolution falls in the range between 50 \AA and 150 \AA in the all observations.

A unit of the observing sequence consisted of successive integrations at four position angles (PA), 0° , $22^\circ.5$, 45° , and $67^\circ.5$, of the half-wave plate. The obtained images were processed using the reduction package for HBS data, which was outlined in Kawabata et al. (1999). Instrumental polarization was derived from unpolarized standard star data obtained almost in each night. The data were averaged in each observation run (typically ~ 10 days for the Okayama 1.88 m telescope and 1-2 months for the other telescopes). The level of instrumental polarization p_{instr} was well expressed by a smooth function of wavelength, and vectorially removed from observed Stokes Q and U spectra. At any run, the stability (1σ) of p_{instr} was less than 0.05 %. The factor of instrumental depolarization was obtained from observation through a Glan-Taylor prism. This observation also gave us the wavelength-dependent PA of the equivalent optical axis of the superachromatic half-wave plate. The zero point of the PA on the sky was de-

termined from observations of strongly polarized standard stars listed in Wolff, Nordsieck, & Nook (1996). The instrumental polarization, the instrumental depolarization, and the zero point of the PA were properly corrected for in the reduction package.

The observations are summarized in Table 1, in which polarization data integrated over the synthetic Johnson V band filter (Bessell 1990) are shown. For the observations with D2 diaphragm, we also show the equivalent widths of the $\text{C}_2(0-0)$ 5165 \AA band in the table. The flux was calibrated using spectrophotometry of some standard stars (Taylor 1984).

3. RESULTS

3.1. Overview

Figure 1 shows the time variation of polarization at the synthetic V band, together with the visual light curve. R CrB experienced three major photometric declines in our observation period. It demonstrates large polarization variability during declines; for example, the polarization angle rotated by more than 30° in 1999 December and the polarization amplitude became over 5 % in 2000 December. On the other hand, R CrB near maximum brightness showed nearly constant polarization (except for on 2001 March 9–12 and August 9). These characteristics are consistent with past observations (e.g., Efimov 1980; Stanford et al. 1988; Clayton et al. 1995). A commonly-accepted explanation for the large polarization during decline is that the unpolarized direct stellar light is heavily obscured by the dust cloud (dust puff) along the line of sight and the visible flux is predominantly scattered light.

However, we detected temporal increase of polarization two times even at maximum brightness stages; the first event was observed on 2001 March 9–12 and the second was on 2001 August 9. In both times, the amplitude of polarization increased by $\Delta p \simeq 0.5 \%$ (Figure 2). Although polarization usually increases accompanied with the onset of major decline phases (Figure 3), we cannot see any significant decline ($\Delta V \gtrsim 0.3$) in the lightcurve around the two events. Also, any remarkable change in flux spectra have not been recognized as shown in Figure 4, and the equivalent width of $\text{C}_2(0-0)$ 5165 \AA absorption band

(Table 1) kept an almost constant value, 22–26 Å, which is consistent with the typical value of R CrB near maximum brightness (17.5–43 Å with an average of 26.5 Å; Clayton et al. 1995). It should be noted, however, that there is possible photometric variations accompanied with the polarimetric variations. The lightcurve shows possible shallow dips (~ 0.1 mag) a few days prior to the polarization events (Figure 2), which could be connected with small dust formation episodes. We will discuss this temporal polarimetric activities after subtraction of the constant polarization component.

3.2. Constant Component of Polarization

It has been known that R CrB shows a nearly constant polarization at maximum brightness. Stanford et al. (1988) averaged the polarization observed in a period when no brightness fluctuations were seen, and derived a constant component of $Q = -0.21$ %, $U = -0.07$ % ($p = 0.22$ %, $\theta = 99^\circ$) as the values averaged over the optical wavelengths. The same values were obtained from averaging subsequent non-decline observations in 1990–1993 (Clayton et al. 1995). Clayton et al. (1997) reported that the observation in 1995 March, before the onset of the decline of 1995, showed a typical Serkowski-type ISP function ($p_{\max} = 0.24 \pm 0.08$ %, $\lambda_{\max} = 0.46 \pm 0.01$ μm , $\theta \sim 100^\circ$) which was in good agreement with the previous estimations. Efimov (1980) assumed the interstellar component of $p_{\max} = 0.2$ % and $\theta = 110^\circ$ from polarization of nearby field stars. Similar technique also gives $p_{\max} = 0.20$ % and $\theta = 97^\circ$ (Biegging et al. 2006).

We averaged our polarization data obtained on 46 nights when R CrB was at maximum brightness stage ($\Delta m_V \leq 0.3$ mag) except those in the periods of the transient polarization. The mean values for Stokes Q and U parameters and their standard deviations in each band are $(Q_B, U_B) = (-0.198 \pm 0.068$ %, -0.020 ± 0.055 %), $(Q_V, U_V) = (-0.203 \pm 0.049$ %, -0.035 ± 0.053 %), $(Q_R, U_R) = (-0.188 \pm 0.044$ %, -0.028 ± 0.056 %), and $(Q_I, U_I) = (-0.161 \pm 0.044$ %, -0.026 ± 0.055 %). Parameters of Serkowski function (Serkowski, Mathewson, & Ford 1975; Whittet et al. 1992) corresponding to those values are derived by a non-linear regression as $p_{\max} = 0.204 \pm 0.046$ %, $\lambda_{\max} = 0.48 \pm 0.27$ μm and $\theta = 94.1 \pm 4.1$. These are consistent with the constant and/or in-

terstellar component derived in previous studies. The constancy of the component over two decades, being much more than the ~ 3.5 yr IR period, allows us to consider that the component is fully interstellar polarization. It is noted that Clayton et al. (1995) found a small variability of polarization up to 0.14 % (possibly correlated with the light curve, at least, for their 1991 data) during the maximum brightness stage. The variability seems rather random, and such an effect would be cancelled out in our averaged values, while they possibly remain in the standard deviations.

4. DISCUSSION

After vectorial subtraction of the constant component from the observations, we obtain variable components of polarization, $p_{\text{var}}(\lambda)$ and $\theta_{\text{var}}(\lambda)$. Their values in synthetic V band are shown in Table 1.

It is known that polarized flux of R CrB is relatively constant since 1968 at the level of $\sim 10^{-3}$ to $10^{-4} F_*$ at any part of declines (Whitney et al. 1992; Clayton et al. 1995, 1997), where F_* is the total stellar flux at maximum brightness stage. Here, the polarized flux is simply derived as

$$f_{\text{pol}} = p_{\text{var}} \times 10^{-0.4\Delta m_V} F_* , \quad (1)$$

where Δm_V is the drop of visual magnitude from maximum $V_{\max} = 6.09$ (see § 1). In our data (Figure 1d), f_{pol} also falls between 10^{-3} and $10^{-4} F_*$ on almost all days both during and out of declines. However, at the epochs of the transient polarization, f_{pol} showed ~ 5 times as much as the typical maximum values, which indicates that the net polarization flux was extraordinarily large.

4.1. Origin of the Transient Polarization

Our polarimetric monitoring brought first detection of the ‘transient polarization’ amounting to 0.5 % for R CrB in the maximum brightness phase. As far as we know, there exists only one observation in which R CrB near maximum brightness showed polarimetric variation larger than 0.2 %: Efimov (1980) found $\Delta p = 0.38 \pm 0.03$ % at $\lambda_{\text{eff}} = 5450$ Å on 1974 August 24 = JD2, 442, 284. Figures 5a and 5b show the time variation of $p_{\text{var}}(\lambda)$ and $\theta_{\text{var}}(\lambda)$ in the periods including the first and second events of the transient polarization. There is no significant wavelength depen-

dence in position angle for both events, compared with the polarization found during decline phase (Figures 6a–c).

Suppose that several clouds exist around R CrB and that they scatter the light from the star. If each cloud was ejected from the photosphere in a random manner and it contains a different polarizing property from one to another, the position angle of the scattered light would be mostly wavelength dependent. The nearly constant θ against λ indicates that the polarization can be ‘effectively’ attributed to scattering by one component. The wavelength dependence of $p_{\text{var}}(\lambda)$ was almost flat in optical wavelengths and quite similar between the two cases. For the event on 1974 August 24, $p(\lambda)$ seems also flat (0.38–0.46 %) in the wavelength range, 3630–7450 Å (Efimov 1980). The similarity in $p_{\text{var}}(\lambda)$ curve suggests an existence of the possible generality in the polarizing mechanism among those three events. Rayleigh scattering by large molecules or smallest solid particles ($\lesssim \lambda/10$) cannot reproduce such wavelength dependence because the scattering coefficient is highly wavelength-dependent ($\propto \lambda^{-4}$). Scattering by free electrons can reproduce a flat $p_{\text{var}}(\lambda)$ curve. However, it is unlikely for R CrB to have a large amount of ionized gas which can produce an observable polarization because the effective temperature of R CrB is not so high ($T_{\text{eff}} \simeq 6900$ K; Schönberner 1975; Asplund et al. 1997). The emission lines which appears in R CrB during declines (e.g., Rao et al. 1999; Rao, Lambert, & Shetrone 2006) are not so strong that spectra at maximum brightness stage have little emission line.

As described in §1, several observational facts suggest that R CrB intermittently ejects dust puffs even at maximum brightness phases. The transient polarization could be naturally explained by a dust puff ejection off the line of sight. The shallow dips in the lightcurve (Figure 2) would support this idea, if we can assume that the dust puff eclipses a small part of the photosphere at the very early (nearest) stage. Single-sized grain of radius $a \simeq 0.1 \mu\text{m}$ shows a peak polarization at optical wavelength and the peak wavelength varies with the grain radius (e.g., Shawl 1975). For flat $p_{\text{var}}(\lambda)$ curve, the dust grains would have a size distribution of a wide range of a .

We performed a calculation of Mie scattering with a simplified model consisting of a point-like

dust cloud and a central star, and estimated the light from the stellar system; that is the sum of an unpolarized direct stellar light and the partially-polarized scattered light. In the calculation we assumed that the dust grains are all spherical amorphous carbon (e.g., Lambert et al. 2001) and adopted the refractive indices of the BE soot (Rouleau & Martin 1991). We also assumed that the cloud is optically-thin, i.e., multiple scattering process is negligible. We set the distance of the cloud $r = 2R_*$ where R_* is the stellar radius ($= 85R_{\odot}$; Feast 1975) and make an estimation of the total mass of dust necessary for explaining the 0.5 % polarization. The results are shown in Figure 7. In the case of forward-scattering (scattering angle $\alpha < 90^\circ$, where α is the angle between the direction of the incident light and that of the scattered one), the $p(\lambda)$ curves gradually decrease with wavelength and they do not fit well the observation. For a right angle scattering and backward-scattering ($\alpha > 90^\circ$) cases, the single-sized grain model fails to reproduce the flat $p(\lambda)$ curve. The size distribution of the carbon dust should range over $\sim 0.13 \mu\text{m}$ in order to produce the flat $p_{\text{var}}(\lambda)$ curve. We here consider a power-law size distribution like a well-known interstellar dust model (Mathis, Rumpl, & Nordsieck 1977; hereafter, MRN). The MRN size distribution is expressed as $n(a) \propto a^{-\beta}$ within $a_{\text{min}} \leq a \leq a_{\text{max}}$, where $\beta = 3.5$, $a_{\text{min}} = 0.005 \mu\text{m}$ and $a_{\text{max}} = 0.25 \mu\text{m}$. Results of the MRN model seem not to contradict the observation in a wide range of scattering angle ($\alpha = 60^\circ\text{--}135^\circ$). This is only an illustrative example. A large choice of parameters (α , a_{min} , a_{max} , β) can yield similar $p_{\text{var}}(\lambda)$ curves. In general, the scattering by grains having various sizes seems a plausible mechanism for the transient polarization. The similarity in the observed $p(\lambda)$ curves between/among two (or three, including Efimov 1980’s event) events suggest that the dependence of $p(\lambda)$ on the scattering angle is not so strong.

A correlation between pulsational phase and the time of decline onset has been found for RY Sgr and V854 Cen which show fairly regular pulsation cycles than R CrB (Pugach 1977; Lawson et al. 1992). Although the correlation is less significant for R CrB itself (Pugach 1977; Goncharova, Kovalchuk & Pugach 1986; Percy et al. 1987; Lawson 1991; Fernie & Seager 1994), it is recently

confirmed by Crause, Lawson, & Henden (2007). These suggest that the condensation of dust is triggered by the stellar pulsation. According to this picture, the appearance of the transient polarization is likely to correlate with the pulsation phase. In our observation, the interval between the two polarization events was 151 ± 1 d. It has been known that R CrB shows a semi-regular pulsation of about 40 d from photometric and spectroscopic observations, for example 38.6 d (Alexander et al. 1972), $P = 39.8$ d (Yudin et al. 2002) and $P = 42.7$ d (Rao et al. 1999). If we assume that the 151 d interval corresponds to four cycles, the length of one cycle is ~ 38 d. This seems a little shorter compared with the pulsation period. However, it is noted again that the pulsation period of R CrB is not coherent. Some shorter periods have been found in a timescale of a few hundred days. Fernie & Seager (1994) found well-developed oscillations with an apparent period of 36.7 ± 0.9 d in late 1992 in the visual light curve; while they also found that the better-defined peaks observed from 1992 through 1993 could be fitted with a single, linear ephemeris of period 35.3 ± 0.2 d. We cannot exclude the possibility that the transient polarization was correlated with the stellar pulsation.

4.2. Size Distribution of Dust

In the previous section, we showed that the wavelength dependence of the transient polarization can be reproduced by light scattering due to the carbon grain with various sizes including grains larger than $\sim 0.13 \mu\text{m}$. However, UV extinction properties at the 1980 decline of R CrB indicate that the dust was grassy or amorphous carbon grain with a size distribution of $a = 0.005\text{--}0.06 \mu\text{m}$ (Hecht et al. 1984). A detailed analysis of extinction curves (Zubko 1997) for three observations of R CrB during declines in 1980–1984 indicated that the size distribution of graphite or amorphous carbon grains has a distinct peak-like form (widths of $\Delta a = 0.002\text{--}0.006 \mu\text{m}$) with typical sizes of $a = 0.03$ through $0.07 \mu\text{m}$. If such small particles scatter the light from the central star, the $p_{\text{var}}(\lambda)$ curve should show a slope of decreasing with wavelength in the optical (Figure 7).

The amplitude of polarization is proportional to inverse square of the distance between the central star and the dust puff, r , while the extinc-

tion depends only on the column density along the line of sight. The information derived from the extinction would be a mean property of the dust clouds along the line of sight toward the star, while the information derived from the polarization would be selectively for the dust close to the central star. Therefore the apparent difference in dust size between the estimate from polarimetry and that from UV extinction may indicate that the size distribution of the dust changes with the distance from the central star. Coyne & Shawl (1973) reported the variability of the wavelength dependence of polarization in 1972 decline of R CrB, and interpreted each observation with scattering by graphite dust of different sizes ranging from 0.05 to $0.10 \mu\text{m}$ in radius. In their results the mean particle size became smaller unsteadily with time. Evans (1985) proposed that the extinction properties of the dust responsible for 1982 decline of the hot RCB star, MV Sgr, can be explained by somewhat large carbon grains ($a \sim 0.2 \mu\text{m}$). Another model applied for the same extinction data also gave a similar result (Zubko 1997). For some extinction data of other RCB stars, he also suggested that the particle size exceeds $a = 0.1 \mu\text{m}$. These facts suggest that the scattering matter consist of discrete clouds with different mean particle sizes (depending on their ages and their distance from the star) even in the same star. If the dust forms near the photosphere, a grain evaporation mechanism might play a role on the change of the size distribution (e.g., Evans 1993). The particle size inferred from our polarimetry suggests that the evolutionary phase of the dust grains causing the transient polarization is more or less the same from that of the dust grains obscuring the stellar flux during deep declines.

4.3. On the Short Timescale of Fading

The transient polarization in 2001 March diminished gradually between March 11 and 13. For the second event, the polarization also diminished within two days. It is remarkable that the decaying timescale of the transient polarization is only ~ 2 days, which is much shorter than the recovery times of the brightness from deep minimum (typically several weeks). If we assume that the scattering geometry keeps similar, the polarized flux approximately depends on the product of intensity of the stellar light at the scattering material

and total scattering cross section. Thus, the amplitude of polarization decreases as the dust cloud goes away from the star (i.e., larger r) or the dust particles are destroyed (i.e., smaller a).

Here we consider the former case. If the decrease of polarization was only due to radial dispersal of dust cloud, the rate of decrease in polarization roughly depends on the radial distance r and the mean expansion velocity of the cloud v_{exp} . The distance can be expressed as $r = R_{\text{df}} + v_{\text{exp}}t$, where R_{df} is the distance between the central star and the place where the dust formation finishes, and t is the time elapsed from the cessation of the dust formation. For simplicity, we assume that the scattering cloud is optically thin. In this case, the polarization amplitude approximately changes as $p(r) = p_c D(r) (R_*/r)^2$, where p_c is a constant and $D(r) = \{1 - (R_*/r)^2\}^{0.5}$ is the finite disk depolarization factor (Cassinelli, Nordsieck, & Murison 1987).³ This function monotonically decreases with r for $r > \sqrt{3/2}R_*$, and the most rapidly decreasing case occurs for nearly $R_{\text{df}} = \sqrt{3/2}R_*$. The observed transient polarization decreased to one fourth within ~ 2 days. These indicate that the dust cloud needs to travel, at least, $1.9R_*$ within two days, i.e., $v_{\text{exp}} \gtrsim 650 \text{ km s}^{-1}$. Thus, if the expansion velocity exceeds 650 km s^{-1} , the dispersal of dust cloud can explain the timescale of the polarization extinction. However, the derived velocity is not consistent with the typical mass loss velocity observed in R CrB. The absorption component of the Na I D or the He I $\lambda 10830$ line are blueshifted by up to -150 to -350 km s^{-1} (e.g., Payne-Gaposchkin 1963; Querci & Querci 1978; Cottrell, Lawson, & Buchhorn 1990; Rao et al. 1999; Clayton, Geballe, & Bianchi 2003). Evolutions of emission line system at the onset of declines suggest that the wind velocity is likely to be lower ($\sim 50 \text{ km s}^{-1}$) at close proximity to the photosphere, $\simeq 1-2R_*$ (Payne-Gaposchkin 1963; Alexander et al. 1972; Clayton 1996). Although higher-velocity wind have been reported in the unusual RCB stars, V854 Cen ($400-1000 \text{ km s}^{-1}$, Clayton et al. 1993; Rao & Lambert 1993), the

³The optical thickness of the cloud might not be practically negligible, which results in depolarization. As the cloud expands, the cloud becomes optically-thin and the polarizing efficiency gradually recovers. Thus, p should be damped more slowly than $D(r) \cdot r^{-2}$ in the vicinity of the star and we obtain the lower-limit of v_{exp} with this method anyhow.

observational facts suggests the ejecta of R CrB is gradually accelerated up to $\sim 200 \text{ km s}^{-1}$ within a few weeks (probably by radiation pressure on dust grains). It is unlikely that the dust puff is accelerated to $v_{\text{exp}} \gtrsim 650 \text{ km s}^{-1}$ within $R \sim 1.2R_*$.

Therefore, the rate of depolarization can hardly be explained only by the radial expansion of the dust puff. If the dust forms actually near the photosphere ($\lesssim 2R_*$), the strong radiation from the central star can evaporate and destroy the dust grains once the possible cooling instability to promote the dust condensation (see §1) terminates. In any case, the rapid disappearance of polarization prefers that the dust grains are formed in an activated region, that is, a region close to the photosphere.

The problem of dust formation in such hostile environments is also under discussion in the field of Wolf-Rayet stars. Some phenomenological similarities with RCB stars have been reported for some late-type WC stars and [WC] PN nuclei (e.g., Williams 1997; Crowther 1997; Veen et al. 1998; Clayton 2001; Kato et al. 2002). Polarization is relatively sensitive to the region close to the light source for some optically-thin systems, and the transient polarization events represent the potential of polarimetry as the probe to the dust formation around such stars.

4.4. Geometry of Mass Loss

Stanford et al. (1988) presented that the PA of polarization in R CrB observed during decline of 1986 was along with data of two previous declines of 1968 and 1972 (Serkowski & Kruszewski 1969; Coyne & Shawl 1973). This suggests that there was a preferred plane (PA $\simeq 30-45^\circ$) in the dust ejection. However, the PAs observed during 1989 and 1993 declines were significantly different from them (Clayton et al. 1995). Clayton et al. (1997) summarized a data set in five declines with polarimetry (from 1971 through 1996) having wavelength information when R CrB was more than 5 mag below maximum brightness, and presented that they well fit to the two opposite sector regions of PA = $15^\circ \pm 15^\circ$ and = $105^\circ \pm 15^\circ$ in QU diagram. They suggested that dust ejection in R CrB has a bipolar geometry consisting of obscuring torus and bipolar lobes. We can see a similar tendency in our data at decline phases (Figure 8). The PA of the largest polarization found dur-

ing the 2000 decline (90° – 100°) falls in the sector regions. The PA in the recovering phase of the 2003 decline (30° – 36°) also falls near the sector regions. These implies that the bipolar geometry for dust ejection directions still exists in R CrB. It is noted that the transient polarization was at 80° – 90° (2001 March) and $\sim 70^\circ$ (2001 August), which lies near or only slightly apart from the edge of the sector regions.

During deep declines a considerable rotation ($\gtrsim 40^\circ$) of the PA with wavelength has been occasionally found in some RCB stars (e.g., Whitney et al. 1992; Clayton et al. 1997). This can be explained by an optical depth effect where a thick torus obscures the central star and thin bipolar lobes act as a reflection nebula (Clayton et al. 1997). On the other hand, for the transient polarization, the rotation of the PA with wavelength is small. It supports the idea that only a single dust puff, which is closest to the photosphere, contributes the transient polarization effectively. The size distribution discussed in §4.2 would reflect the real properties of the newborn grains selectively.

Ohnaka et al. (2001) carried out K -band speckle interferometric observations of R CrB on 1996 October 1 ($V = 7$) and 1999 September 28 ($V = 10.61$) and suggested that the large dust shell (with an inner boundary at $r = 82R_*$ and 920 K) has a rather isotropic distribution, at least, in a scale of larger than $\sim 300R_*$. The authors also introduced a newly formed dust cloud close to the star ($r = 4.5R_*$ and 1200 K) to fit both the visibility and the spectral energy distribution simultaneously. Asplund et al. (1997) gave an analysis of SED with a model atmosphere and suggested that the IR excess could be explained by recently formed, hot dust grains ($\sim 2000\text{K}$) amounting to a total mass of $\sim 10^{-11} M_\odot$. Some extinction models for RCB stars suggested that the total mass (gas+dust) per ejection event were 10^{-9} – $10^{-7} M_\odot$ (Feast 1986; Fadeyev 1988; Clayton et al. 1992) although these could be affected by uncertainties in r , ϕ (opening angle of the dust puff), and the gas-to-dust ratio. Yudin et al. (2002) derived a mean dust formation rate of $3.1 \times 10^{-9} M_\odot \text{ yr}^{-1}$ with a radiative transfer modeling. Our Monte Carlo simulation (see Appendix) suggests that the dust puff off the line of sight can produce a polarization of $\simeq 0.5\%$ when it has a mass of $\gtrsim 9 \times 10^{-13} M_\odot$ and an opening angle of $\gtrsim 40^\circ$ for $r \sim 2R_*$.

The actual mass should be highly model dependent. However, the lower-limit of the dust mass is still much less than the mean dust formation rate ($\sim 10^{-9} M_\odot \text{ yr}^{-1}$), and we conclude that the amplitude of polarization in the transient polarization events would be consistent with the random ejection model in which dust puffs are formed in the close vicinity of the stellar atmosphere.

5. SUMMARY AND CONCLUSION

We carried out spectropolarimetric monitoring of R CrB from 1998 January to 2003 September. The constant component of polarization derived by Stanford et al. (1988) and confirmed by Clayton et al. (1995) still existed in our observational period. In addition, we discovered a temporal increase of polarization up to $\simeq 0.5\%$ at maximum brightness stage in 2001 March and August. It is likely that dust puff which was ejected off the line of sight produced the transient polarization. Shallow declines (~ 0.1 mag) were marginally found a few days prior to the polarization events, which would support this idea if we can assume that the dust puff eclipsed a part of the photosphere at the very early stage. The flatness in $p_{\text{var}}(\lambda)$ curve of the transient polarization, which was a common property for both two cases, suggested that the size distribution of the dust was not like a δ -function (as the results of UV–optical extinction studies) but rather wide, e.g., a well-known model of interstellar dust (MRN size distribution). We suggest that the size distribution evolves with the age or the distance from the star. The fading timescale ($\sim 2 \pm 0.5$ days) of the polarization is fairly rapid compared with the recovering rate of brightness from deep declines. It cannot be interpreted by a simple dissipation due to radial expansion of the dust puff at the expansion velocity of $\sim 200 - 350 \text{ km s}^{-1}$, even in the case where the dust formation occurred at $r \sim 2 R_*$. Higher expansion velocity or some mechanism to destroy the dust grains should be needed.

So far we have not detected a possible increasing part of the transient polarization, which would be important to discuss the process and the site of the dust formation around RCB stars. Further spectropolarimetric monitoring of RCB stars near maximum brightness will bring a valuable information of a dust formation and destruction pro-

cesses in a hostile circumstellar environment.

We thank G. C. Clayton, the referee, for helpful suggestions. We are grateful to T. Cho, H. Iwamatsu, S. Hamasaka, N. Hirakata, R. Hirata, K. Homma, K. Hoshino, T. Karube, N. Kobayashi, M. Kondoh, S. Masuda, Y. Nakamura, S. Nakayama, A. Okazaki, I. Ota, M. Saito, T. Sakurai, R. Suzuki, C. Tokoku, K. Yoshioka for their kind supports to the observation. We also thank to the staff members of Dodaira Observatory and Okayama Astrophysical Observatory of NAOJ for technical supports, especially to Y. Norimoto, H. Shibasaki and K. Okita. We are indebted to the variable star observations from the VSNET and AAVSO database contributed by observers worldwide for the light curve of R CrB. Data reduction/analysis was in part carried out on the “sb” computer system operated by the Astronomical Data Analysis Center (ADAC) and Subaru telescope of NAOJ. NAOJ is an interuniversity research institute of astronomy operated by the Ministry of Education, Culture, Sports, Science and Technology. This work was supported by a Grant-in-Aid from the Ministry of Education, Culture, Sports, Science and Technology of Japan (No. 17684004).

A. MONTE-CARLO SIMULATION OF POLARIZATION BY DUST PUFF

Monte Carlo method is a useful tool to solve problems including multiple scattering of light since it requires only a few assumptions and it can be applied for many kinds of complicated geometries and particles. The details in application of Monte Carlo method for light scattering process is described in, e.g., Warren-Smith (1983), and Hillier (1991).

As seen in Figure 9, we consider the Cartesian coordinate, (x, y, z) . We define that the origin is the center of the star. The stellar radius is 1, i.e., the coordinate is normalized by the stellar radius. The direction of the earth is $\mathbf{e} = (0, 0, 1)$. The shape of the dust puff is a part of geometrically-thin spherical shell with a radius of r and an opening angle of ϕ from the origin. The center of the dust puff, \mathbf{r} , is located in the x - z plane. These enable us to investigate the depolarization effect due to finite solid angle of the photosphere in the neighborhood of the star, which is a different point from Code & Whitney (1995)'s. Optical depth of the cloud along \mathbf{r} is τ_0 . For simplicity, we neglect geometrical thickness of the shell. The scattering angle, that is, the angle between \mathbf{r} and \mathbf{e} , is α .

In our Monte Carlo simulation, more than a million photons are emitted from random sites on the stellar surface toward random directions. All released photons have the same intensity, which means that rim darkening effect is neglected. When they meet the cloud, some penetrate, some are absorbed by, and the others are scattered by dust grains in the cloud. The scattered photons are partially polarized and emitted again toward a new direction according to a phase function $\mathbf{R}(\alpha)$. We adopt a single peaked Henyey-Greenstein function (White 1979) as the phase function:

$$\mathbf{R}(\alpha) = \frac{3}{4} \begin{pmatrix} P_1 & P_2 & 0 & 0 \\ P_2 & P_1 & 0 & 0 \\ 0 & 0 & P_3 & -P_4 \\ 0 & 0 & P_4 & P_3 \end{pmatrix}, \quad (\text{A1})$$

and,

$$P_1 = \frac{1 - g^2}{(1 + g^2 - 2g \cos \alpha)^{3/2}}, \quad (\text{A2})$$

$$P_2 = -p_l \frac{1 - \cos^2 \alpha}{1 + \cos^2 \alpha} P_1, \quad (\text{A3})$$

$$P_3 = \frac{2 \cos \alpha}{1 + \cos^2 \alpha} P_1, \quad (\text{A4})$$

$$P_4 = -p_c \frac{1 - \cos^2 \alpha_f}{1 + \cos^2 \alpha_f} P_1, \quad (\text{A5})$$

$$\alpha_f = \alpha(1 + 3.13s \exp[-7\alpha/\pi]), \quad (\text{A6})$$

where g is an asymmetric parameter (ranging from 0 for isotropic scattering to 1 for forward-throwing), p_l and p_c are the maximum linear and circular polarization, respectively, and s is the skew factor ($= 1$ in almost all cases). Three parameters α , g , and p_l , are related with the linear polarization. g varies with a wavelength and a mean size of dust. White (1979) investigated the dependency of g on wavelength for a well-known model of interstellar graphite dust. We used his values, lacking a better alternative for a mixture of cosmic grains having various sizes. Referring to Figure 2 of his paper, we adopt $g = 0.46$ at 5500 \AA . We also obtain the albedo $\omega = 0.61$ at 5500 \AA from the same figure. The p_l is set to 0.51 (Code & Whitney 1995). Although the single peaked Henyey-Greenstein phase function is not well approximated at longer wavelength region and for back-scattering cases (White 1979), the difference can be negligible in our cases, i.e., $x = 2\pi a/\lambda \lesssim 1$ and $\alpha \leq 135^\circ$. More details of our calculation will be described in a preparing paper (Ikeda & Seki 2007).

A.1. Size and Mass of Dust Puff

In this section, we give a rough estimation for the size and mass of dust puff responsible for the amplitude of the transient polarization ($p_{\text{var}} \simeq 0.5\%$) using the Monte-Carlo method. In Table 2 we summarized the

results at 5500 Å for both $r = 2R_*$ and $20R_*$ cases. Since the wavelength dependence is expected to be small for the dust model, they can be considered as typical values in the optical region. It is obvious that the models of $\alpha' = 135^\circ$ (backward scattering) cannot produce $p > 0.5$, where α' is the scattering angle at the cloud center. Figure 10 shows the relations of τ_0 vs. ϕ satisfying polarization of 0.5%. To obtain the results of $p \simeq 0.5\%$, we need (i) $\tau_0 \gtrsim 0.5$ and $\phi \gtrsim 40^\circ$ for $r = 2R_*$, or (ii) $\tau_0 \gtrsim 0.5$ and $\phi \gtrsim 20^\circ$ for $r = 20R_*$. The cloud at larger distance can produce $p = 0.5\%$ with smaller optical thickness and smaller opening angle because the depolarization effect due to finite solid angle of the photosphere become small. However, larger mass is needed for large r . We can estimate the total mass of the dust puff as

$$M_d = \frac{4\pi}{3} \rho \langle a^3 \rangle \frac{\tau_0}{\langle \sigma_{\text{ext}} \rangle} r^2 \Omega \quad (\text{A7})$$

$$\simeq 2.7 \times 10^{-12} \left(\frac{\tau_0}{1.0} \right) \left(\frac{r}{R_*} \right)^2 \left(1 - \cos \frac{\phi}{2} \right) M_\odot, \quad (\text{A8})$$

where ρ is the bulk density of dust grains, $\langle a^3 \rangle$ and $\langle \sigma_{\text{ext}} \rangle$ are the averaged cubic radius and averaged cross section of extinction per a dust particle, respectively, and Ω is solid angle of the puff seen from the star. In Equation A8 we adopted $\langle a^3 \rangle = 3.80 \times 10^{-18} \text{ cm}^3$ and $\langle \sigma_{\text{ext}} \rangle = 1.42 \times 10^{-12} \text{ cm}^2$ (White 1979), $\rho = 2.2 \text{ g cm}^{-3}$ (Evans 1993). We have $M_d \simeq 9 \times 10^{-13} \tau_0 M_\odot$ for the $r = 2R_*$ case ($\phi = 48^\circ$), and $3 \times 10^{-11} \tau_0 M_\odot$ for the $r = 20R_*$ case ($\phi = 28^\circ$).

REFERENCES

- Alexander, J. B., Andrews, P. J., Catchpole, R. M., Feast, M. W., Lloyd Evans, T., Menzies, J. W., Wisse, P. N. J., & Wisse, M. 1972, *MNRAS*, 158, 305
- Asplund, M., & Gustafsson, B. 1996, in *ASP Conf. Ser. Vol. 96, Hydrogen-Deficient Stars*, eds. C. S. Jeffery and U. Heber (San Francisco: ASP), 39
- Asplund, M., Gustafsson, B., Kiselman, D., & Eriksson, K. 1997, *A&A*, 318, 521
- Bessell, M. S. 1990, *PASP*, 102, 1181
- Biegging, J. H., Schmidt, G. D., Smith, P. S., & Oppenheimer, B. D. 2006, *ApJ*, 639, 1053
- Cassinelli, J. P., Nordsieck, K. H., & Murison, M. A. 1987, *ApJ*, 317, 290
- Clayton, G. C., Whitney, B. A., Stanford, S. A., & Drilling, J. S. 1992, *ApJ*, 397, 652
- Clayton, G. C., Lawson, W. A., Whitney, B. A., & Pollacco, D. L. 1993, *MNRAS*, 264, L13
- Clayton, G. C., Lawson, W. A., Cottrell, P. L., Whitney, B. A., Stanford, S. A., & de Ruyter, F. 1994, *ApJ*, 432, 785
- Clayton, G. C., Whitney, B. A., Meade, M. R., Babler, B., Bjorkman, K. S., & Nordsieck, K. H. 1995, *PASP*, 107, 416
- Clayton, G. C. 1996, *PASP*, 108, 225
- Clayton, G. C., Bjorkman, K. S., Nordsieck, K. H., & Zellner, N. E. 1997, *ApJ*, 476, 870
- Clayton, G. C. 2001, *Ap&SS*, 275, 143
- Clayton, G. C., Geballe, T. R., & Bianchi, L. 2003, *ApJ*, 595, 412
- Clayton, G. C., Geballe, T. R., Herwig, F., Fryer, C., & Asplund, M. 2007, *ApJ*, 662, 1220
- Code, A. D., & Whitney, B. A. 1995, *ApJ*, 441, 400
- Cottrell, P. L., Lawson, W. A., & Buchhorn, M. 1990, *MNRAS*, 244, 149
- Coyne, G. V., & Shawl, S. J. 1973, *ApJ*, 186, 961
- Coyne, G. V. 1974, *IBVS*, No. 914
- Crause, L. A., Lawson, W. A., & Henden, A. A. 2007, *MNRAS*, 375, 301
- Crowther, P. A. 1997, *MNRAS*, 290, L59
- de Laverny, P., Mékarnia, D. 2004, *A&A*, 428, L13
- Efimov, Yu. S. 1980, *Bull. Crimean Astrophys. Obs.*, 61, 88
- Efimov, Yu. S. 1990, *AZh*, 67, 494
- Evans, A. 1993, *The Dusty Universe* (New York: Ellis Horwood)
- Evans, A., Whittet, D. C. B., Davies, J. K., Kilkenny, D., & Bode, M. F. 1985, *MNRAS*, 217, 767
- Fadeyev, Y. A. 1986, in *Hydrogen Deficient Stars and Related Objects*, eds. K. Hunger, D. Schönberner, N. Kameswara Rao (Dordrecht: Reidel), 441
- Fadeyev, Y. A. 1988, *MNRAS*, 233, 65
- Feast, M. W. 1975, in *IAU Symp. No. 67, Variable Stars and Stellar Evolution*, eds. V. E. Sherwood and L. Plaut (Dordrecht: Reidel), 129
- Feast, M. W. 1986, in *Hydrogen Deficient Stars and Related Objects*, eds. K. Hunger, D. Schönberner, N. Kameswara Rao (Dordrecht: Reidel), 151
- Feast, M. W. 1997, *MNRAS*, 285, 339
- Feast, M. W. 2000, in *IAU Symp. 177, The Carbon Star Phenomenon*, ed. R. F. Wing (Dordrecht: Kluwer), 207
- Feast, M. W., Carter, B. S., Roberts, G., Marang, F., & Catchpole, R. M. 1997, *MNRAS*, 285, 317
- Feast, M. W., & Glass, I. S. 1973, *MNRAS*, 161, 293
- Fernie, J. D., & Seager, S. 1994, *PASP*, 106, 1138
- Forrest, W. J., Gillett, F. C., & Stein, W. A. 1972, *ApJ*, 178, L129
- Goncharova, R. I., Kovalchuk, G. U., Pugach, A. F. 1983, *Astrophysics*, 19, 161

- Hecht, J. H., Holm, A. V., Donn, B., & Wu, C. C. 1984, *ApJ*, 280, 228
- Hillier, D. J. 1991, *A&A*, 247, 455
- Ibe, I. J., Tutukov, A. V., & Yungelson, L. R. 1996, *ApJ*, 456, 750
- Ikeda, Y., & Seki, M. 2007, in preparation.
- Kato, T., Haseda, K., Takamizawa, K., & Yamaoka, H. 2002, *A&A*, 393, L69
- Kawabata, K. S., et al. 1999, *PASP*, 111, 898
- Lambert, D. L., Rao, N. K., Pandey, G., & Ivans, I. I. 2001, *ApJ*, 555, 925
- Lawson, W. A. 1991, *MNRAS*, 253, 625
- Lawson, W. A., Cottrell, P. L., Gilmore, A. C., & Kilmartin, P. M. 1992, *MNRAS*, 256, 339
- Loreta, E. 1934, *Astr. Nach.*, 254, 151
- Mathis, J. S., Ruml, W., & Nordsieck, K. H. 1977, *ApJ*, 217, 425
- Ohnaka, K., et al. 2001, *A&A*, 380, 212
- Ohnaka, K., et al. 2003, *A&A*, 408, 553
- O'Keefe, J. A. 1939, *ApJ*, 90, 294
- Payne-Gaposchkin, C. 1960, *ApJ*, 138, 320
- Percy, J. R., Carriere, L. E. M., & Fabro, V. A. 1987, *AJ*, 93, 200
- Pugach, A. F. 1977, *IBVS*, 1277
- Querci, M., & Querci, F. 1978, *A&A*, 70, L45
- Rao, N. K., et al. 1999, *MNRAS*, 310, 717
- Rao, N. K., & Lambert, D. L. 1993, *AJ*, 105, 1915
- Rao, N. K., Lambert, D. L., & Shetrone, M. D. 2006, *MNRAS*, 370, 941
- Rosenbush, A. É. & Rosenbush, V. K. 1990, *IBVS*, 3439
- Rosenbush, A. É. 2001, *Astrophysics*, 44, 78
- Rouleau, F. & Martin, P. G., 1991, *ApJ*, 377, 526
- Saio, H., & Jeffery, C. S. 2002, *MNRAS*, 333, 121
- Schönberner, D. 1975, *A&A*, 44, 383
- Serkowski, K., & Kruszewski, A. 1969, *ApJ*, 155, L15
- Serkowski, K., Mathewson, D. S., & Ford, V. L. 1975, *ApJ*, 196, 261
- Shawl, S. J. 1975, *AJ*, 80, 595
- Soker, N., & Clayton, G. C. 1999, *MNRAS*, 307, 993
- Stanford, S. A., Clayton, G. C., Meade, M. R., Nordsieck, K. H., Whitney, B. A., Murison, M. A., Nook, M. A., & Anderson, C. M. 1988, *ApJ*, 325, L9
- Stein, W. A., Gaustad, J. E., Gillett, F. C., & Knacke, R. F. 1969, *ApJ*, 155, L3
- Taylor, B. J. 1984, *ApJS*, 54, 259
- Trammell, S. R., Dinerstein, H. L., & Goodrich, R. W. 1994, *AJ*, 108, 984
- Veen, P. M., van Genderen, A. M., van der Hucht, K. A., Sterken, C., & Dominik, C. 1998, *A&A*, 329, 199
- Warren-Smith, R. F. 1983, *MNRAS*, 205, 337
- Wickramasinghe, N. C. 1973, *Light Scattering Functions for Small Particles with Applications in Astronomy* (London: Adam Hilger)
- White, R.L. 1979, *ApJ*, 229, 954
- Whitney, B. A., & Clayton, G. C., Schulte-Ladbeck, R. E., & Meade, M. R. 1992, *AJ*, 103, 1652
- Whitney, B. A., Balm, S. P., & Clayton, G. C. 1993, in *ASP Conf. Ser. Vol. 45, Luminous High-Latitude Stars*, ed. D. Sasselov (San Francisco: ASP), 105
- Whittet, D. C. B., Martin, P. G., Hough, J. H., Rouse, M. F., Bailey, J. A., & Axon, D. J. 1992, *ApJ*, 386, 562
- Williams, P. M. 1997, *Ap&SS*, 251, 321
- Woitke, P., Goeres, A., & Sedlmayr, E. 1996, *A&A*, 313, 217

Wolff, M. J., Nordsieck, K. H., & Nook, M. A.
1996, AJ, 111, 856

Yudin, B. F., Fernie, J. D., Ikhsanov, N. R.,
Shenavrin, V. I., & Weigelt, G. 2002, A&A, 394,
617

Yudin, R. V., Evans, A., Barrett, P., Albinson, J.
S., Davies, J. K., & Hutchinson, M. G. 2003,
A&A, 412, 405

Zubko, V. G. 1997, MNRAS, 289, 305

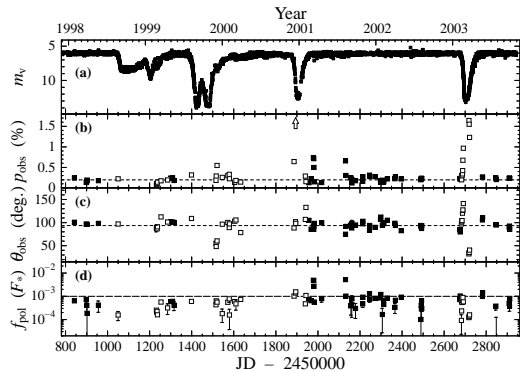


Fig. 1.— Time variation of polarimetric properties of R CrB. This figure shows (a) visual magnitude from VSNET, (b) observed polarization amplitude, (c) its position angle, and (d) polarized flux at synthetic V band against Julian date. The visual magnitude data are from VSNET database. Polarization data are shown by filled squares for observations at maximum brightness stage ($\Delta m_V \leq 0.3$) and by open squares during declines ($\Delta m_V > 0.3$), with observational error (1σ). The horizontal lines in (b) and (c) denote the constant component of polarization at V band (see §3.2). The arrow in (b) indicates that there are data points much larger than the shown range. The polarized flux is derived from variable component of polarization and magnitude drop (see §3.3). In the maximum brightness stage R CrB generally showed a nearly constant polarization, while it showed significant temporal variation in 2001 March and August.

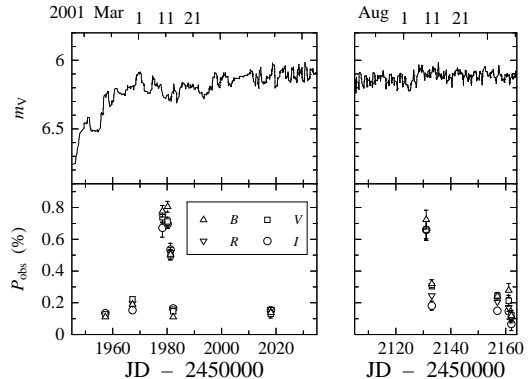


Fig. 2.— Time variation of visual magnitude and observed polarization in the epochs including the transient polarization events. For the lightcurve we show smoothed (17 point running-mean) AAVSO validated magnitudes, which includes a wealth of data points (about four times more than VSNET ones). Triangles, squares, inverse triangles, and circles denote the amplitude of observed polarization in synthetic B , V , R , and I bands, respectively. It seems that there is temporal photometric variations of ~ 0.1 mag a few days prior to the polarization peaks, which could be connected with small dust formation episodes.

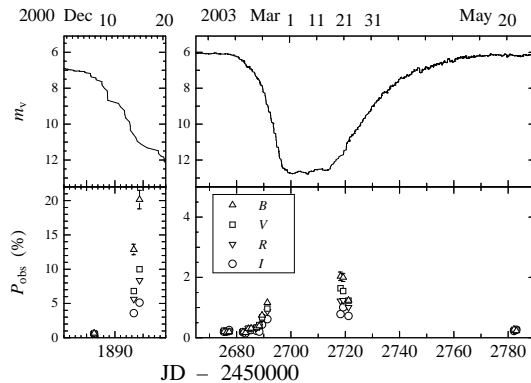


Fig. 3.— Same as Figure 2 during 2000-2001 and 2003 declines. The data are plotted with the same manner in Figure 2. The amplitude of polarization increases as the star fades. Bluer polarization increases more rapidly than red one, which is consistent with the past polarimetry. The ratio of polarization amplitude to Δm_V was higher in 2000–2001 decline than in 2003 decline.

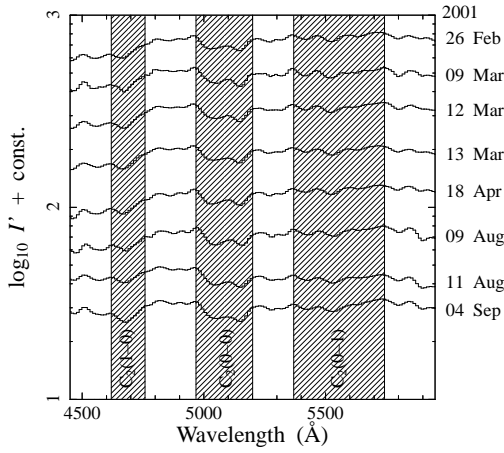


Fig. 4.— Sample spectra of R CrB in the maximum brightness stage including the periods of the transient polarization. The system response (instrument+telescope) is corrected but airmass effect is not corrected in those spectra. The date of observation is indicated at right side of each spectrum. Hatched area denotes the molecular bands (C_2). No significant variation is seen in the period.

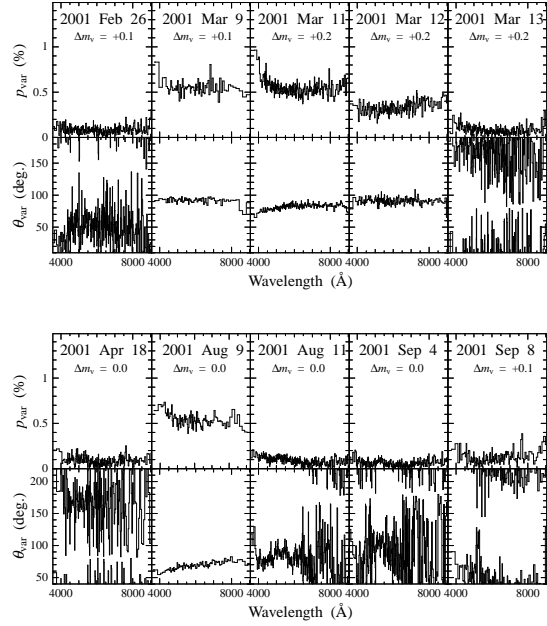


Fig. 5.— Temporal variation in the wavelength dependence of the variable component of polarization at maximum brightness phases: Upper combined figure shows polarization amplitude and its position angle around the first event of the transient polarization (2001 March) and the lower one shows the second one (2001 August). The data are binned to a constant photon noise of 0.04%. The date of observation and the V magnitude below the maximum $m_V = 6.09$ are indicated in each upper panel.

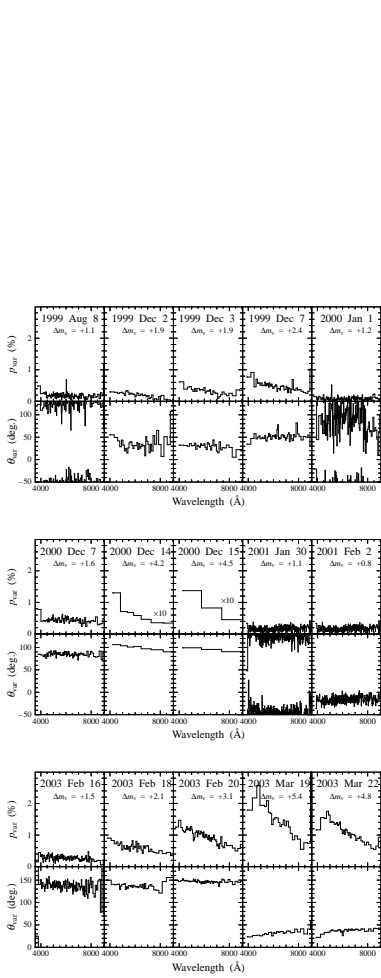


Fig. 6.— Same as Figure 5 during decline phases. The polarization during decline phase generally has a wavelength dependence; p_{var} is larger at bluer wavelengths.

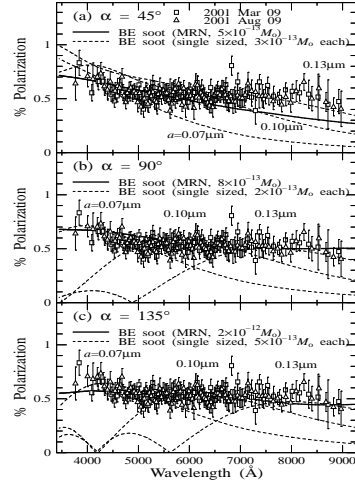


Fig. 7.— Samples of wavelength dependence of polarization calculated with Mie scattering theory. From top to bottom, we show them in the case of the scattering angle $\alpha = 45^\circ$, 90° and 135° , respectively. The dust model is an amorphous carbon (BE soot; Rouleau & Martin 1991). Open squares and triangles are variable components of polarization observed on 2001 March 9 and on August 9, respectively. Dashed lines denote the results for scattering by single-sized ($a = 0.07, 0.10, 0.13 \mu\text{m}$) grains. Thick solid lines are results for a mixture of grains of an inverse power-law size distribution ($n(a) \propto a^{-3.5}$) having lower and upper cutoffs at $0.005 \mu\text{m}$ and $0.25 \mu\text{m}$, respectively (Mathis, Rumpl, & Nordsieck 1977). In this model we assume an optically-thin case and the dust mass corresponds to $r = 2R_*$ indicated in the parentheses should be considered as approximated values.

TABLE 1
POLARIMETRY OF R CRB.

Date <i>yyyymmdd</i>	JD 2450000+	Δm_V^a 6.11+	Tel. ^b	Diaph. ^c	CCD ^d	Exp. sec	C_2 5165 ^e (EW) Å	Observed polarization ^f		Variable component ^f		Pol. flux ^g $10^{-5} F_*$
								p_V (%)	θ_V (deg.)	p_V (%)	θ_V (deg.)	
19980128	0842.32	-0.06	D36	D1	T	1200	—	0.24 ± 0.01	100.8 ± 1.8	0.06 ± 0.02	124.3 ± 6.5	64 ± 16
19980325	0898.20	-0.00	D36	D2	T	1440	18	0.13 ± 0.02	96.7 ± 4.9	0.07 ± 0.02	181.4 ± 9.1	73 ± 22
19980328	0901.23	-0.03	D36	D1	T	1680	—	0.17 ± 0.02	96.1 ± 3.3	0.04 ± 0.02	179.7 ± 13.4	41 ± 21
19980329	0902.19	-0.08	D36	D1	T	792	—	0.19 ± 0.03	96.2 ± 4.1	0.02 ± 0.03	168.9 ± 46.3	19 ± 32
19980522	0956.07	-0.12	D36	D1	T	1260	—	0.18 ± 0.02	98.3 ± 3.3	0.04 ± 0.02	168.0 ± 15.0	42 ± 21
19980824	1050.01	+0.40	O74	D1	T	960	—	0.22 ± 0.01	96.9 ± 1.3	0.02 ± 0.01	117.0 ± 11.8	16 ± 7
19990222	1232.23	+1.82	D36	D1	T	3200	—	0.08 ± 0.02	87.4 ± 7.4	0.13 ± 0.02	189.2 ± 4.3	25 ± 4
19990223	1233.22	+1.80	D36	D1	T	2880	—	0.10 ± 0.02	88.8 ± 5.3	0.11 ± 0.02	190.1 ± 4.6	21 ± 3
19990225	1235.23	+1.67	D36	D1	T	2880	—	0.11 ± 0.01	86.5 ± 3.5	0.11 ± 0.01	193.1 ± 3.5	23 ± 3
19990227	1237.19	+1.60	D36	D1	T	4200	—	0.14 ± 0.01	90.8 ± 2.9	0.07 ± 0.01	193.0 ± 5.7	16 ± 3
19990316	1254.18	+0.85	D36	D1	T	1800	—	0.17 ± 0.01	112.3 ± 1.4	0.12 ± 0.01	156.0 ± 2.1	56 ± 4
19990416	1285.16	+0.38	D36	D1	T	1800	—	0.19 ± 0.02	101.2 ± 3.3	0.05 ± 0.02	150.5 ± 14.2	32 ± 15
19990501	1300.06	+0.11	D36	D1	T	1680	—	0.24 ± 0.01	102.0 ± 1.7	0.06 ± 0.01	128.1 ± 5.8	59 ± 13
19990510	1309.19	+0.09	O74	D1	T	1440	—	0.25 ± 0.02	101.2 ± 1.6	0.07 ± 0.01	122.8 ± 6.4	61 ± 13
19990517	1316.21	+0.11	O74	D1	T	1680	—	0.18 ± 0.02	100.4 ± 3.2	0.05 ± 0.02	159.8 ± 12.1	41 ± 17
19990808	1399.01	+1.09	D36	D1	S	1500	—	0.32 ± 0.02	108.9 ± 1.8	0.17 ± 0.02	126.7 ± 3.0	60 ± 8
19991202	1515.34	+1.87	D36	D1	S	1200	—	0.18 ± 0.04	55.2 ± 5.9	0.25 ± 0.04	28.1 ± 4.4	43 ± 7
19991203	1516.34	+1.87	D36	D1	S	1200	—	0.29 ± 0.03	48.2 ± 4.0	0.37 ± 0.04	31.1 ± 3.1	64 ± 6
19991207	1520.33	+2.42	D36	D1	S	1920	—	0.55 ± 0.02	60.3 ± 1.2	0.51 ± 0.02	49.3 ± 1.3	56 ± 2
20000101	1545.33	+1.16	D36	D1	S	2400	—	0.26 ± 0.03	96.6 ± 3.7	0.05 ± 0.03	103.4 ± 17.2	18 ± 10
20000127	1571.30	+0.72	D36	D1	S	1560	—	0.30 ± 0.03	100.4 ± 2.3	0.11 ± 0.03	111.4 ± 6.7	55 ± 13
20000203	1578.30	+0.64	D36	D1	S	640	—	0.33 ± 0.04	89.4 ± 3.5	0.14 ± 0.04	81.1 ± 8.6	78 ± 24
20000204	1579.26	+0.55	D36	D1	S	1680	—	0.22 ± 0.02	97.1 ± 2.4	0.03 ± 0.02	117.4 ± 21.8	16 ± 12
20000229	1604.19	+0.42	D36	D1	S	2176	—	0.13 ± 0.02	103.1 ± 5.2	0.09 ± 0.02	171.8 ± 8.2	60 ± 14
20000306	1610.22	+0.53	D36	D1	S	2560	—	0.18 ± 0.03	105.5 ± 5.7	0.08 ± 0.04	154.1 ± 13.1	48 ± 22
20000329	1633.15	+0.54	D36	D1	S	2080	—	0.14 ± 0.02	78.4 ± 4.2	0.12 ± 0.02	25.6 ± 5.0	73 ± 13
20001207	1886.35	+1.64	O36	D1	S	1500	—	0.64 ± 0.04	88.4 ± 2.0	0.44 ± 0.04	85.5 ± 2.8	102 ± 10
20001214	1893.35	+4.18	O36	D1	S	2800	—	6.81 ± 0.31	102.0 ± 1.4	6.61 ± 0.31	102.2 ± 1.4	138 ± 6
20001215	1894.35	+4.52	O36	D1	S	2400	—	9.98 ± 0.42	98.4 ± 1.2	9.78 ± 0.42	98.5 ± 1.3	155 ± 7
20010130	1940.30	+1.13	O74	D2	T	5600	20	0.29 ± 0.03	107.0 ± 2.9	0.13 ± 0.03	127.1 ± 6.2	47 ± 11
20010202	1943.32	+0.84	O74	D1	T	2240	—	0.15 ± 0.03	132.9 ± 5.6	0.23 ± 0.03	164.2 ± 3.8	108 ± 14
20010216	1957.34	+0.26	O36	D2	S	1680	30	0.13 ± 0.01	104.9 ± 3.0	0.10 ± 0.01	171.5 ± 3.9	74 ± 11
20010226	1967.29	+0.15	O36	D2	S	2400	23	0.22 ± 0.02	85.6 ± 2.2	0.07 ± 0.02	51.7 ± 6.9	64 ± 16
20010309	1978.30	+0.13	O36	D2	S	1800	23	0.74 ± 0.03	92.6 ± 1.1	0.53 ± 0.03	91.7 ± 1.6	487 ± 28
20010311	1980.17	+0.07	O36	D1	S	3840	—	0.71 ± 0.03	85.8 ± 1.2	0.52 ± 0.03	82.2 ± 1.6	475 ± 25
20010312	1981.24	+0.11	O36	D2	S	3640	25	0.50 ± 0.03	92.1 ± 1.6	0.30 ± 0.03	90.2 ± 2.6	269 ± 26
20010313	1982.22	+0.08	O36	D2	S	2000	25	0.15 ± 0.01	98.3 ± 2.3	0.06 ± 0.01	176.6 ± 5.5	57 ± 11
20010418	2018.09	+0.03	O36	D2	S	1440	24	0.13 ± 0.02	99.6 ± 5.0	0.08 ± 0.02	177.0 ± 8.3	79 ± 23
20010809	2131.05	+0.00	O36	D2	S	900	22	0.66 ± 0.06	74.8 ± 2.5	0.52 ± 0.06	67.4 ± 3.1	520 ± 56
20010811	2133.06	+0.02	O36	D2	S	1200	24	0.30 ± 0.02	91.7 ± 2.0	0.10 ± 0.02	85.3 ± 5.9	102 ± 22
20010904	2156.97	-0.04	O36	D2	S	1080	28	0.24 ± 0.02	94.5 ± 2.5	0.04 ± 0.02	92.5 ± 15.6	39 ± 23
20010908	2161.04	+0.05	O36	D2	S	960	29	0.21 ± 0.03	88.4 ± 4.6	0.05 ± 0.03	51.3 ± 20.4	44 ± 31
20010909	2162.03	+0.06	O36	D2	S	1080	29	0.12 ± 0.03	98.4 ± 6.4	0.09 ± 0.03	179.9 ± 8.9	79 ± 26
20010926	2178.95	-0.02	O36	D2	S	1200	27	0.18 ± 0.02	94.8 ± 2.9	0.03 ± 0.02	185.4 ± 17.1	30 ± 19

TABLE 1—*Continued*

Date <i>yyyymmdd</i>	JD 2450000+	Δm_V^a 6.11+	Tel. ^b	Diaph. ^c	CCD ^d	Exp. sec	C_2 5165 ^e (EW) Å	Observed polarization ^f		Variable component ^f		Pol. flux ^g $10^{-5} F_*$
								p_V (%)	θ_V (deg.)	p_V (%)	θ_V (deg.)	
20011030	2212.90	-0.01	O36	D2	S	960	29	0.16 ± 0.01	97.4 ± 2.7	0.05 ± 0.01	176.1 ± 9.1	47 ± 14
20011031	2213.89	+0.00	O36	D2	S	1120	29	0.27 ± 0.02	102.9 ± 2.3	0.09 ± 0.02	122.2 ± 6.7	91 ± 22
20011201	2245.36	+0.12	O36	D2	S	1600	22	0.31 ± 0.01	83.9 ± 1.2	0.14 ± 0.01	67.8 ± 2.6	131 ± 12
20011202	2246.36	+0.07	O36	D2	S	1200	20	0.29 ± 0.02	93.9 ± 2.6	0.08 ± 0.02	91.5 ± 9.0	75 ± 19
20011227	2271.35	-0.05	O36	D2	S	3000	25	0.28 ± 0.01	89.8 ± 1.3	0.08 ± 0.01	76.6 ± 4.2	81 ± 12
20020122	2297.36	-0.04	O36	D2	S	1200	18	0.18 ± 0.01	106.9 ± 1.6	0.09 ± 0.01	154.7 ± 3.2	85 ± 10
20020124	2299.37	-0.05	O36	D2	S	1080	19	0.14 ± 0.01	111.9 ± 2.4	0.12 ± 0.01	164.6 ± 2.8	120 ± 11
20020131	2306.31	-0.03	O36	D2	S	1800	25	0.19 ± 0.01	94.4 ± 2.0	0.02 ± 0.01	189.9 ± 22.6	17 ± 14
20020206	2312.28	+0.01	O36	D2	S	2160	29	0.14 ± 0.01	99.3 ± 2.4	0.07 ± 0.01	175.2 ± 5.1	68 ± 11
20020207	2313.26	-0.01	O36	D2	S	2160	28	0.17 ± 0.01	97.6 ± 1.6	0.04 ± 0.01	174.6 ± 5.8	44 ± 10
20020224	2330.27	-0.12	O74	D2	S	360	26	0.22 ± 0.02	105.1 ± 2.6	0.08 ± 0.02	140.1 ± 7.8	84 ± 21
20020401	2366.31	-0.01	O36	D2	S	1260	22	0.22 ± 0.02	98.6 ± 1.9	0.03 ± 0.02	125.0 ± 12.9	33 ± 15
20020403	2368.22	-0.01	O36	D2	S	2700	23	0.27 ± 0.01	93.8 ± 0.6	0.07 ± 0.01	90.6 ± 2.6	67 ± 7
20020501	2396.11	+0.04	O36	D2	S	2880	29	0.22 ± 0.01	82.4 ± 1.1	0.09 ± 0.01	47.6 ± 2.5	92 ± 8
20020803	2489.97	-0.02	O36	D2	S	900	14	0.21 ± 0.02	93.9 ± 2.6	0.01 ± 0.02	24.5 ± 51.1	10 ± 18
20020804	2490.98	-0.01	O36	D2	S	900	25	0.23 ± 0.01	90.7 ± 1.0	0.04 ± 0.01	67.4 ± 6.1	40 ± 9
20020805	2492.04	-0.01	O36	D2	S	900	24	0.22 ± 0.02	91.4 ± 2.1	0.03 ± 0.02	62.4 ± 16.6	29 ± 16
20020806	2492.99	-0.00	O36	D2	S	1260	25	0.23 ± 0.01	87.3 ± 1.5	0.06 ± 0.01	58.7 ± 6.1	64 ± 13
20020807	2493.96	+0.01	O36	D2	S	972	25	0.23 ± 0.01	93.1 ± 1.0	0.03 ± 0.01	80.6 ± 7.7	30 ± 8
20030204	2675.33	+0.07	O36	D2	S	1800	30	0.23 ± 0.01	84.4 ± 1.5	0.08 ± 0.01	53.8 ± 3.8	76 ± 11
20030205	2676.31	+0.06	O36	D2	S	1440	29	0.22 ± 0.01	79.7 ± 1.4	0.11 ± 0.01	46.4 ± 2.5	103 ± 10
20030206	2677.25	+0.04	O36	D2	S	1600	29	0.21 ± 0.01	84.8 ± 1.0	0.07 ± 0.01	45.2 ± 3.2	72 ± 7
20030211	2682.33	+0.66	O36	D2	S	3200	27	0.21 ± 0.02	97.2 ± 1.8	0.02 ± 0.01	132.8 ± 24.6	9 ± 7
20030212	2683.29	+0.70	O36	D2	S	2880	27	0.20 ± 0.01	101.1 ± 1.6	0.05 ± 0.01	148.0 ± 6.0	24 ± 6
20030213	2684.32	+0.76	O36	D2	S	2400	25	0.30 ± 0.01	103.7 ± 0.9	0.12 ± 0.01	118.8 ± 2.2	59 ± 5
20030214	2685.31	+0.95	O36	D2	S	4000	24	0.30 ± 0.01	104.4 ± 0.8	0.12 ± 0.01	121.0 ± 1.9	54 ± 3
20030216	2687.34	+1.48	O36	D2	S	2400	23	0.34 ± 0.01	120.4 ± 0.8	0.27 ± 0.01	138.9 ± 1.1	67 ± 3
20030217	2688.30	+1.69	O36	D2	S	2400	22	0.42 ± 0.04	126.5 ± 2.6	0.38 ± 0.04	141.0 ± 2.8	79 ± 9
20030218	2689.34	+2.08	O36	D2	S	2400	24	0.67 ± 0.02	127.6 ± 0.8	0.62 ± 0.02	136.4 ± 0.9	89 ± 3
20030220	2691.28	+3.09	O36	D2	S	3200	32	0.97 ± 0.02	141.2 ± 0.6	1.00 ± 0.02	147.1 ± 0.5	57 ± 1
20030319	2718.26	+5.44	O36	D2	S	9600	10	1.64 ± 0.06	32.5 ± 0.8	1.77 ± 0.06	29.7 ± 0.8	12 ± 0.4
20030320	2719.23	+5.17	O36	D2	S	10800	13	1.55 ± 0.04	35.5 ± 0.7	1.66 ± 0.04	32.3 ± 0.7	14 ± 0.3
20030322	2721.19	+4.83	O36	D2	S	9600	10	1.23 ± 0.04	40.6 ± 0.8	1.31 ± 0.04	36.3 ± 0.7	16 ± 0.5
20030522	2782.12	+0.02	O36	D2	T	4140	24	0.26 ± 0.02	105.7 ± 2.6	0.10 ± 0.02	129.3 ± 5.9	103 ± 24
20030523	2783.02	+0.03	O36	D2	T	3200	24	0.27 ± 0.01	110.8 ± 1.5	0.14 ± 0.02	135.9 ± 2.6	141 ± 15
20030725	2845.97	+0.04	O36	D2	S	700	44	0.24 ± 0.01	95.7 ± 1.6	0.04 ± 0.01	100.4 ± 10.4	38 ± 12
20030727	2848.09	+0.05	O36	D2	S	552	41	0.21 ± 0.01	94.9 ± 2.1	0.00 ± 0.01	164.1 ± 550.3	1 ± 124
20030926	2908.96	-0.07	O36	D2	S	1800	18	0.24 ± 0.01	90.4 ± 1.5	0.05 ± 0.01	67.8 ± 7.6	50 ± 13
20030928	2910.92	-0.05	O36	D2	S	1080	20	0.24 ± 0.02	92.5 ± 1.8	0.04 ± 0.02	79.5 ± 11.3	38 ± 15
20030929	2911.92	-0.04	O36	D2	S	960	18	0.24 ± 0.01	85.6 ± 1.6	0.08 ± 0.01	57.0 ± 3.9	77 ± 13

^aVisual magnitude averaged for all data within ±2.5 days in VSNET database.^bD36, O36 and O74 denote 0.91 m at Dodaira, 0.91 m at Okayama and 1.88 m at Okayama, respectively.

^cD1: 1.4 mm ϕ circle, D2: 0.2 mm \times 1.4 mm rectangle.

^dT and S denote TI CCD and SITe CCD, respectively.

^eThe equivalent width of the C₂ (0 – 0) 5165 Å band is measured between 4970 Å and 5200 Å for D2 observations.

^fObserved polarization is considered as a vectorial summation of a constant component and a variable component (see text).

^gPolarized flux $p_{\text{var}} \times 10^{-0.4\Delta m_V} F_*$

r	α	ϕ	% polarization			
			$\tau_0 = 0.3$	$\tau_0 = 1.0$	$\tau_0 = 3.0$	$\tau_0 = 5.0$
$2 R_*$	45°	20°	0.035	0.081	0.118	0.122
		30°	0.074	0.175	0.250	0.259
		45°	0.151	0.351	0.497	0.511
		60°	0.232	0.533	0.742	0.768
	90°	20°	0.042	0.100	0.144	0.148
		30°	0.092	0.218	0.311	0.321
		45°	0.191	0.453	0.640	0.663
		60°	0.306	0.718	1.014	1.051
	135°	20°	0.011	0.026	0.038	0.039
		30°	0.024	0.058	0.083	0.087
		45°	0.052	0.122	0.174	0.180
		60°	0.086	0.200	0.287	0.297
$20 R_*$	45°	10°	0.030	0.073	0.110	0.115
		20°	0.116	0.278	0.415	0.434
		30°	0.243	0.579	0.856	0.892
		45°	0.471	1.089	1.588	1.634
	90°	10°	0.028	0.069	0.104	0.109
		20°	0.111	0.269	0.404	0.422
		30°	0.239	0.577	0.865	0.901
		45°	0.489	1.169	1.732	1.804
	135°	10°	0.005	0.012	0.018	0.019
		20°	0.020	0.049	0.073	0.077
		30°	0.045	0.109	0.164	0.171
		45°	0.100	0.242	0.361	0.376

Table 2: Monte Carlo simulation of polarization due to scattering by dust puff